On the enigmatic disappearance of Rauber's layer

Jessica van Leeuwen[a,b], Pisana Rawson[c], Debra K. Berg[a], David N. Wells[a], and Peter L. Pfeffer[a,c,1]

[a]Animal Reproduction Group, Agresearch Ruakura, 3214 Hamilton, New Zealand; [b]Department of Biomedical, Molecular and Cellular Biology, Waikato University, 3240 Hamilton, New Zealand; and [c]School of Biological Sciences, Victoria University of Wellington, 6012 Wellington, New Zealand

Edited by Denis Duboule, University of Geneva, Geneva, Switzerland, and approved May 29, 2020 (received for review February 2, 2020)

The polar trophoblast overlays the epiblast in eutherian mammals and, depending on the species, has one of two different fates. It either remains a single-layered, thinning epithelium called "Rauber's layer," which soon disintegrates, or, alternatively, it keeps proliferating, contributing heavily to the population of differentiating, invasive trophoblast cells and, at least in mice, to the induction of gastrulation. While loss of the persistent polar trophoblast in mice leads to reduced induction of gastrulation, we show here that prevention of the loss of the polar trophoblast in cattle results in ectopic domains of the gastrulation marker, *BRACHYURY*. This phenotype, and increased epiblast proliferation, arose when Rauber's layer was maintained for a day longer by countering apoptosis through BCL2 overexpression. This suggests that the disappearance of Rauber's layer is a necessity, presumably to avoid excessive signaling interactions between this layer and the subjacent epiblast. We note that, in all species in which the polar trophoblast persists, including humans and mice, ectopic polar trophoblast signaling is prevented via epiblast cavitation which leads to the (pro)amniotic cavity, whose function is to distance the central epiblast from such signaling interactions.

polar trophoblast | amniotic cavity | epiblast

Embryos of all eutherian mammals develop through a blastocyst stage consisting of a shell of trophoblast cells enclosing a cavity containing a mesenchymal mass of cells attached at one pole. The trophoblast forms the fetal part of the placenta (1). The aggregate of cells on the interior of the blastocyst is the inner cell mass (ICM) and will give rise to the epiblast and hypoblast. The hypoblast (sometimes termed "primitive endoderm") cells underlay the epiblast and migrate around the inside of the cavity to develop into yolk sac epithelium. The epiblast is pluripotent and forms the embryo proper, as well as contributing to extraembryonic membranes.

In the advanced blastocyst, we thus encounter a trilaminar configuration at the pole where the ICM developed: The outermost layer is polar trophoblast, in the middle is a disk of epiblast cells, and beneath this is the "visceral" hypoblast. The rest of the embryo is bilaminar, composed of mural/parietal ("wall") trophoblast underlain by parietal hypoblast. Subsequently, blastocysts of different mammalian species diverge greatly as far as the polar trophoblast is concerned. In 1875, Rauber (2) described, in early rabbit blastocysts, that a thin layer of cells (the "Deckschicht") covering the epiblast subsequently dissolves. Koellicker (3) recognized this Deckschicht to be (polar) trophoblast and named it Rauber's layer. That term has since been used to refer to the polar trophoblast layer in all those mammals in which it is lost. The list of such animals is large and covers representatives from 10 orders spread among all superordinal mammalian groupings apart from Xenarthra (*SI Appendix*, Table S1, and see Fig. 6*B*). In all these species, loss of Rauber's layer results in the epiblast being directly exposed to the maternal (uterine) environment. This exposure is terminated upon the upward (i.e., toward the polar side) folding, and sealing, of the edges of the epithelialized epiblast, to form the amniotic cavity.

In "non-Rauber's layer" mammals, which populate all four superordinal mammalian groupings (eight orders; *SI Appendix*, Table S1, and see Fig. 6*B*), the polar trophoblast not only remains intact but, in some species, shows the greatest proliferative capacity of all trophoblast regions. In the case of mice and guinea pigs (Rodentia), in vitro experiments indicated that early trophoblast is dependent on mitogenic or differentiation-inhibitive signals emanating from the ICM/epiblast, explaining why trophoblast expansion is restricted to the pole region (4, 5). In other species with a persisting polar trophoblast, an intermediate situation between polar trophoblast-only proliferation and loss is seen. In rhesus monkeys and humans (higher primates), and in bats, proliferation of mural and polar trophoblast occurs, but is more intense on the epiblast pole, which is the side that implants first (6–11).

The anatomical consequence of these two different trajectories of the polar trophoblast is that, in Rauber's layer species, the superficial surface of the epiblast becomes exposed to the uterine environment, whereas, in the other species, the epiblast remains shielded by the persistent polar trophoblast. This may have functional consequences for epiblast development in that, firstly, endometrial contact or direct maternal signaling may occur in one scenario but not the other.

Secondly, loss of the polar trophoblast in Rauber's layer species removes signaling interactions between the epiblast and this tissue. Yet, in mice, which retain their polar trophoblast, such signaling is crucial in patterning of the epiblast. In mice, continued proliferation of the polar trophoblast generates a mass of cells (the extraembryonic ectoderm), from which the ectoplacental cone and invasive trophoblast giant cells derive (12). Following cavitation, an "egg cylinder" is formed with a cup-shaped epiblast projecting into the blastocyst cavity joined at its rim to the rim of the "inverted cup"-shaped extraembryonic ectoderm. At this circular epiblast–trophoblast boundary, convertase proteases and BMP4/8b signaling molecules diffuse from the trophoblast into the epiblast, while FGF4 and NODAL signals reciprocate, eventually leading to the setting up of the

Significance

Trophoblast contributes to mammalian placenta formation, but it also has an earlier function in gastrulation induction within the embryonic epiblast. We show here that gastrulation induction occurs ectopically if the central area of the epiblast disc contacts the trophoblast for too long. Hence the central epiblast must be shielded from trophoblast influence. We propose that this novel "shielding" principle holds for all mammals and is achieved either through the removal of the trophoblast (Rauber's layer) overlaying the epiblast or by the formation of a cavity within the epiblast (the proamniotic cavity) thereby distancing the central epiblast from the trophoblast.

Author contributions: J.v.L. and P.L.P. designed research; J.v.L., P.R., D.K.B., D.N.W., and P.L.P. performed research; J.v.L. and P.L.P. analyzed data; and P.L.P. wrote the paper.

The authors declare no competing interest.

This article is a PNAS Direct Submission.

[1]To whom correspondence may be addressed. Email: peter.pfeffer@vuw.ac.nz.

This article contains supporting information online at https://www.pnas.org/lookup/suppl/doi:10.1073/pnas.2002008117/-/DCSupplemental.

First published June 29, 2020.

gastrulation organizer in the (posterior) epiblast rim (detailed in *Discussion*). Notably, by failing to maintain the polar trophoblast, for example, by genetic ablation of the gene *Elf5*, which is required for survival of the extraembryonic ectoderm, gastrulation fails (13).

This brings us immediately to the question as to how gastrulation may be induced in those mammals that do not preserve the polar trophoblast, that is, in Rauber's layer species. To answer this, it is necessary to first describe the events surrounding Rauber's layer disappearance. In most Rauber's layer species, the epiblast proliferates to form a multilayered disk or ball of loosely arranged cells, covered outwardly by a very thin contiguous spread of trophoblast cells that is Rauber's layer, and, on the inside, by visceral hypoblast (1). The dissolution of Rauber's layer, whether it be gradual or abrupt, represents a breach of the permeability seal surrounding the blastocyst cavity and would lead to the loss of turgidity and potential collapse of the embryo. To prevent this, the epiblast forms junctional complexes between cells at the edge of the epiblast disk and the neighboring mural trophoblast cells, and then between the epiblast cells themselves, prior to the appearance of gaps in Rauber's layer (14–17). This epithelialization and cell-linking process leads to a flattening out of the epiblast disk, and, by the time Rauber's layer disintegrates, a seamless connection between the mural trophoblast and epiblast epithelia has been established (14, 18, 19). Thus, once the polar trophoblast (Rauber's layer) is gone, the rim of the epiblast touches the mural trophoblast, which is similar to the mouse embryo (if projected onto a flat surface), except that extraembryonic ectoderm (polar trophoblast) has been substituted with the mural trophoblast in Rauber's layer species. It follows that, if the reciprocal trophoblast–epiblast signaling mechanism leading to mouse gastrulation is conserved in Rauber's layer species, then the rim of mural trophoblast surrounding the epiblast disk may be functionally equivalent to the mouse extraembryonic ectoderm abutting the mouse epiblast (19).

Indeed, comparisons of molecular markers in Rauber's layer species such as cattle (19), pigs (20, 21), rabbits (22, 23), and an Eulipotyphlan (insectivore), the musk shrew (23), do provide evidence of at least a partial conservation of the mouse's reciprocal circuitry. The convertase *FURIN* is expressed not only in Rauber's layer but also in the adjacent ring of mural trophoblast in cattle, pigs, rabbits, and musk shrews (19, 23, 24). *NODAL* in these species is, similarly to the mouse (25), more highly expressed in the (posterior) rim region of the epiblast prior to gastrulation (19, 21, 23). *BMP4* expression is less well conserved. In pregastrulation mouse and musk shrew embryos, *BMP4* is restricted to the extraembryonic ectoderm or circumferential rim of mural trophoblast, respectively (23, 26), but, in cattle and rabbits, it is instead seen in a circumferential ring of parietal hypoblast and weakly in epiblast (19, 22).

Apart from a role in the induction of gastrulation, signaling from the mouse polar trophoblast has also been linked to the establishment of the anterior–posterior axis. The future anterior end of the embryo is set up by a thickened area of the visceral hypoblast that underlies the epiblast. This area is termed the AVE (anterior visceral endoderm) and secretes inhibitors of NODAL into the overlying epiblast (27, 28). These inhibitors effect that NODAL activity, and thus the induction of gastrulation and primitive streak formation (which defines the future posterior end of the embryo) is restricted to the opposite rim of the epiblast (29). The AVE itself is formed via directed migration of hypoblast cells under the guidance of the DVH (distal visceral hypoblast) (30). The latter, in turn, is believed to be induced in the visceral hypoblast at the distal apex of the egg cylinder once the epiblast has proliferated sufficiently to bring the DVH out of the inhibitory signaling reach of the polar trophoblast (31, 32). An off-center thickening of part of the visceral hypoblast corresponding to the AVE seems to be a universal feature of eutherian mammals, originally termed "Randzone" in rabbits (3) and "protochordal plate" in musk shrews (33) but, nowadays, anterior visceral hypoblast (AVH) in cattle and pigs (19, 21) or anterior marginal crescent in rabbits (34). The expression of the NODAL-inhibitors LEFTY and CERBERUS1 (CER1) in the AVH is highly conserved across mammalian species (19, 23); however, in contrast to mice, it is unknown whether trophoblast is (indirectly) involved in AVH formation (19).

To summarize, in all eutherian mammals, the polar trophoblast forms. Subsequently, it either persists or disappears. The polar trophoblast is critical for embryonic patterning when it persists (in the mouse), yet Rauber's layer species do not seem to require the polar trophoblast for such patterning nor for a shielding from maternal influences. This brings us to the intriguing question as to why a tissue, that is already present and can be put to such productive use (as in the mouse), is simply discarded in so many mammalian species. Could it be that the dismantling of Rauber's layer is not inconsequential but rather of functional importance? We decided to test this idea by delaying Rauber's layer disappearance in cattle embryos.

Results

Mechanism of Rauber's Layer Disappearance. The two most likely mechanisms for the rupture and disappearance of Rauber's layer are either that its constituent cells stop replicating, and thus differential expansion of epiblast and Rauber's layer causes its rupture, or that the trophoblast cells die. We therefore measured proliferation and apoptosis in embryos during the stages when holes start appearing in Rauber's layer. Cell counting in sections of embryos stained for the proliferation marker phospho-HISTONE H3 (Fig. 1*A*) revealed that there was no difference in proliferation between Rauber's layer trophoblast and the mural trophoblast adjacent to or distant from the embryonic disk, in RL stage 1 ("Rauber's layer-intact" stage; $n = 5$) or VH stage 2 ("visceral hypoblast visible" stage; $n = 7$) embryos (Fig. 1*B*). Proliferation within Rauber's layer remained constant, with a third of cells positive for the proliferation marker. The fraction of proliferating cells also did not differ significantly from that seen in the underlying epiblast. At these stages, the single-layered epithelial sheet of cells that is Rauber's layer is expanding in only two dimensions, whereas proliferation in the underlying epiblast takes place in three dimensions to form the multilayered epiblast seen in VH stage 2 and AVH stage 3 ("AVH visible" stage) embryos. Given the similar proportion of proliferating cells, this means that the epiblast cannot outgrow the overlying trophoblast along the tangential plane, making it unlikely that insufficient Rauber's layer expansion contributes to its rupture.

This leaves cell death as the likely cause for the disintegration of Rauber's layer. Morphological studies in rabbits and horses have revealed the appearance of vacuoles in Rauber's layer cells concomitant with the appearance of gaps in this layer, suggesting cell death (14, 15). In cattle, cell disintegration in Rauber's layer has been reported (35). We used antibodies against active (cleaved) caspase 3, which is the main executioner caspase during apoptosis, to detect programmed cell death in stages 1 to 3 embryos. Active caspase 3 staining was rarely seen in mural trophoblast and hypoblast tissue. Apoptosis was also not detected in the intact Rauber's layer at stage 1 (Fig. 1*C*), but was seen in about 40% of the cells in more advanced embryos which already showed signs of Rauber's layer disintegration (Fig. 1 *D–F*). In the epiblast, apoptosis was seen in a couple of cells (2.1% of the epiblast cells, $n = 4$ embryos serially sectioned; Fig. 1 *C* and *F*). We conclude that programmed cell death as opposed to lack of proliferation leads to the gaps and eventual disappearance of Rauber's layer.

A Transgenic Model for Delaying the Disappearance of Rauber's Layer. From the above results, we reasoned that, by inhibiting apoptosis, it should be possible to delay the destruction of Rauber's

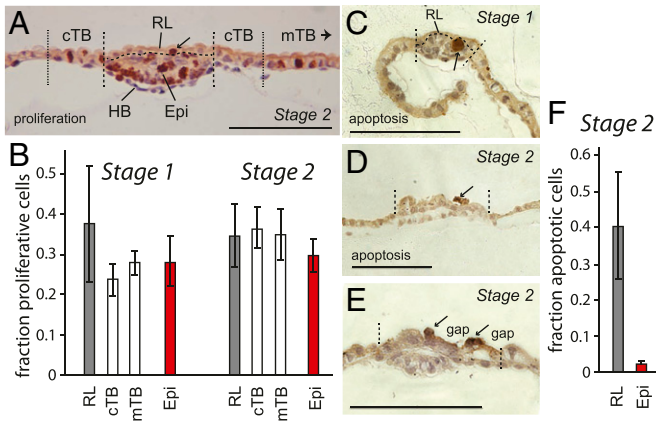

Fig. 1. The mechanism of Rauber's layer disintegration. (*A*) Section of a VH stage 2 embryo stained for proliferative cells using anti-phospho-Histone H3 antibody (#06-570; Upstate Biotechnologies) and counterstained with hematoxylin and eosin. (*B*) Mitotic cells were counted in serial sections of RL stage 1 ($n = 5$), and stage 2 ($n = 7$) embryos within the regions delineated by the dashed lines shown in *A*, with circumferential trophoblast (cTB) defined as TB cells within five cell diameters of the embryonic disk, and mural T as all TB cells more than 10 cell diameters distant from the disk. Mitotic cells as fraction of all cells within each tissue are graphed with error bars representing SEM. (*C*–*E*) Cross-sections of three embryos stained for apoptosis using cleaved caspase-3 (Asp175) antibody (#9661; Cell Signaling Technology). Disk borders are shown by stippled lines. (*C*) RL stage 1 embryo (0.32 mm, 55-μm disk) with a clump of apoptotic cells in the epiblast. (*D*) Stage 2 embryo (0.67 mm, 117-μm disk) and (*E*) second stage 2 embryo (0.61 mm, 90-μm disk), showing gaps in Rauber's layer and Rauber's layer cells surrounding the gaps undergoing apoptosis. Arrows indicate examples of stained cells. Epi, epiblast; mTB, mural trophoblast. (Scale bars, 100 μm.) (*F*) Apoptotic cells counted in stage 2 embryos ($n = 4$) as for *B*.

layer. To achieve this, we built a DNA construct (Fig. 2*A*) designed to express the anti-apoptotic protein BCL2 driven by the *CAG* enhancer. We have previously shown the *CAG* enhancer to yield robust expression in cattle embryos (36, 37). Successful protein production could be monitored via the addition of *GFP* linked to the 5′ end of *BCL2* using a self-processing *TaV2A* element, which results in equimolar GFP and BCL2 protein production (38). Addition of a cocistronic *IRES-puromycin* cassette to the *CAG-BCL2-TaV2A-GFP* expression unit ensured that puromycin-resistant transfected cells would express *BCL2*. This strategy allowed us to isolate bovine primary fibroblast cell lines overexpressing *BCL2* 100- to 400-fold, relative to background levels (Fig. 2*B*). *BCL2*-overexpressing cell lines displayed a high resistance to ultraviolet (UV)-induced apoptosis (Fig. 2*C*). Four cell lines of *BCL2*-overexpressing and two lines of *LacZ* (control: *pCAG-LacZiPuro*) cell lines were used to create transgenic embryos via somatic cell nuclear transfer.

There was no significant difference between *BCL2* and control *LacZ* transgenic embryos in in vitro development to day 5 morula or day 7 blastocyst stages (*SI Appendix*, Table S2), even though *BCL2* messenger RNA (mRNA) was robustly overexpressed at levels as high as housekeeping genes (Fig. 2*D*). BCL2 protein production was inferred via fluorescence of the cotranslated GFP reporter (Fig. 2 *F* and *G*). *BCL2* and control *LacZ* transgenic day 7 blastocysts were then cotransferred into recipient cows and recovered on days 13 to 15 (day 0 = fertilization). At these stages, *BCL2* was expressed, relative to the three housekeepers, at slightly lower levels than at the blastocyst stage, but still, on average, at 50-fold–higher levels than in control transgenic embryos (Fig. 2*E*). GFP fluorescence allowed for easy distinction of *BCL2* and *LacZ* transgenics (Fig. 2 *H* and *I*).

No significant difference ($P = 0.8$) could be detected between the number of *BCL2* and *LacZ* embryos recovered per cow (mean recovery rates of 51% and 53%, respectively), taking into consideration individual cow variation via statistical restricted maximum likelihood analysis (*SI Appendix*, Fig. S1).

Effect of BCL2 Overexpression on the Mural Trophoblast. Proliferation of mural trophoblast causes the increase in embryo length seen from around day 11, and this increase in embryo length provides a reliable age-independent indication of developmental stage (19). No difference in average embryo length could be detected at days 13 to 15 between *BCL2* and control embryos (Fig. 3*A*), suggesting that BCL2 overexpression had no discernible effect on mural trophoblast proliferation/survival or, by inference, on developmental stage. Secondly, expression of the trophoblast differentiation marker *ASCL2* peaks from days 13 to 15 (37, 39), and can be used to assess appropriate stage-specific development of the trophoblast. No difference in *ASCL2* expression between *BCL2* and control embryos was seen at any of the days (Fig. 3*B*). In sum, we conclude that mural trophoblast development and proliferation is appropriate for age, in embryos overexpressing *BCL2*.

Effect of BCL2 Overexpression on the Epiblast. In normal embryos, there is close synchrony between trophoblast and epiblast development, as indicated by a high correlation ($R^2 = 0.81$) between the logarithms of embryo and epiblast length (19). However, when comparing embryo to epiblast length in *BCL2* embryos to that in *LacZ* embryos, we found a highly significant difference ($P = 0.0002$). *BCL2* epiblasts were 35% longer than control epiblasts for any given embryo length (Fig. 3*C*). To exclude the possibility that the size difference was caused by abnormally small epiblasts in *LacZ* embryos, we also compared

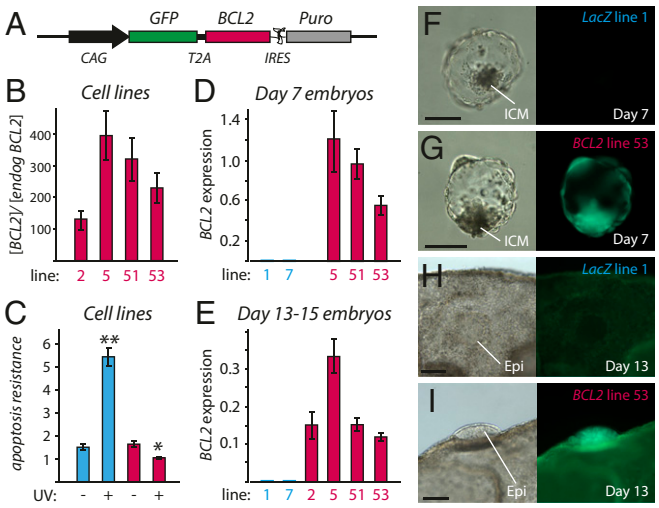

Fig. 2. Creating a transgenic model to examine the effect of Rauber's layer disappearance. (*A*) DNA construct for overexpressing cattle *BCL2*. *Puro*, *puromycin*. (*B*) Expression of transgenic plus endogenous *BCL2*, in relation to endogenous *BCL2*, in four *BCL2*-overexpressing embryonic fibroblast primary cell lines, as measured by real-time RT-PCR. Bars denote SEM. (*C*) Apoptosis resistance assay, showing induction of caspase 3/7 activity, normalized to amount of protein (arbitrary units), in response to UV exposure. Experiment performed in triplicate. Blue bars, *LacZ* overexpressing line (#1); red bars, *BCL2*-overexpressing line (#53); $^{**}P < 0.001$; $^{*}P < 0.01$. (*D*) *BCL2* expression, normalized to the geomean of housekeeping genes *GAPDH*, *CYCLOPHILLIN* and *HPRT*, in day 7 (D7) *BCL2* and control *LacZ* transgenic embryos (*BCL2* line 5, $n = 2$; line 51, $n = 6$; line 53, $n = 2$; *LacZ* line 1, $n = 2$; line 7, $n = 1$; n refers to number of pools of six to eight embryos). (*E*) Normalized *BCL2* expression in days 13 to 15 embryos (*BCL2* line 2, $n = 4$; line 5, $n = 9$; line 51, $n = 16$; line 53, $n = 17$; *LacZ* line 1, $n = 20$; line 7, $n = 10$). (*F*–*I*) Brightfield and fluorescent images of representative D7 and D13 transgenic embryos. Error bars denote SEM. (Scale bars, 100 μm.)

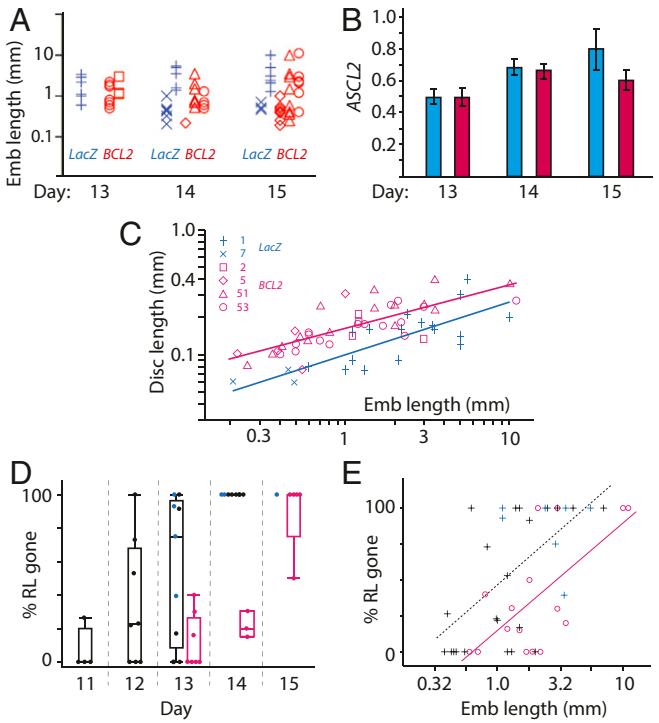

Fig. 3. Effect of *BCL2* overexpression in cattle embryos (Emb). (*A*) Embryo length (logarithmic scale) for *BCL2* (red) and *LacZ* (blue) transgenic embryos retrieved between embryonic days 13 and 15, with different transgenic cell lines used for nuclear transfer indicated by symbols shown in *C*. No significant difference was found between *BCL2* and cotransferred *LacZ* embryos. (*B*) Trophoblast marker *ASCL2* expression, normalized to the geomean of three housekeeping genes, was not found to be different between *BCL2* (red) and *LacZ* (blue) embryos at days 13 to 15. (*C*) Embryonic disk length in relation to embryo length (log scales) with a regression line fitted for each group. *BCL2* embryos had significantly longer embryonic discs ($P < 0.0001$) and were, on average, 35% longer compared to cotransferred *LacZ* embryos. (*D*) In WT (black dots) and *LacZ* (blue dots) transgenic embryos, Rauber's layer starts disappearing from day 11 and is gone by day 14 with the percentage of trophoblast surface area overlying the epiblast shown. In contrast, in *BCL2* embryos (red dots), Rauber's layer is intact in the majority of D13 embryos and only fully gone from D15. The box and whisker overlays display quartiles. (*E*) The delay in Rauber's layer disappearance corresponds to a 2.4-fold increase in embryo length. Trend lines are red for *BCL2*, and black stippled for (*LacZ* + WT) with $R^2 = 0.44$ for *BCL2*, $R^2 = 0.36$ for *LacZ*. Red circles, *BCL2*; blue plus signs, *LacZ*; black plus signs, WT embryos.

both types of transgenic embryos to nontransgenic control embryos, which we had analyzed previously (19). *LacZ* and wild-type (WT) embryos did not differ significantly, whereas *BCL2* embryos had 20% larger epiblasts (ANCOVA [analysis of covariance]–Tukey, $P = 0.0023$). The cause of the precociously large epiblast was not determined; however, the size increase could have placed the overlying trophoblast layer under increased tensional strain, potentially causing the precocious rupture of Rauber's layer instead of achieving our goal of extending the maintenance of this layer.

Effect of BCL2 Overexpression on Maintaining Rauber's Layer. We estimated the timing and extent of Rauber's layer disintegration using complete serial sections through the embryonic disk of transgenic embryos and staining for OCT4 protein so as to unambiguously distinguish epiblast from trophoblast. We also compared our results to the nontransgenic (WT) control embryos mentioned above. Rauber's layer starts disintegrating from day 11 in control embryos (Fig. 3*D*). By day 13, controls had lost 57 ± 14% of Rauber's layer, whereas *BCL2* embryos had lost only 11 ± 5.7%, a highly significant difference ($P = 0.01$, ANOVA). By day 14, all controls (*LacZ* and WT) had lost all of Rauber's layer, whereas all *BCL2*-overexpressing embryos had lost less than a third of this layer, with one embryo retaining half of Rauber's layer right up to day 15 (Fig. 3*D*). The delay in Rauber's layer disintegration was approximately 1 d (Fig. 3*D*).

We tested whether a delay in Rauber's layer was also seen when using embryo length as a measure of developmental age. This is particularly informative, as embryo length was unaffected in *BCL2*-overexpressing embryos. Such an analysis revealed that *BCL2* transgenic embryos contained, on average, 26% more Rauber's layer than controls at any given length or, conversely, were 2.4× longer at an equivalent Rauber's layer disintegration state ($P < 0.01$, ANCOVA; Fig. 3*E*). We, and others, had previously shown that the increase in embryo length between days 11 and 16 is twofold per day (40, 41). We therefore can conclude that overexpression of BCL2 delays the disintegration of Rauber's layer by slightly more than 1 d, whether judged by chronological age or by total embryo length. Interestingly, Rauber's layer is eventually lost when overexpressing BCL2. We examined whether this is due to cell death signaling from the epiblast to Rauber's layer via the type I extrinsic apoptotic pathway, which cannot be inhibited by BCL2 overexpression. We found no evidence for this. Of the death receptors, only *FAS* and *TNFRSF10b*/*DR-5* were expressed in trophoblast, but their ligands, FASL and TRAIL, were not expressed in the underlying epiblast (*SI Appendix*, Table S3) (42). We suspect the eventual rupturing of Rauber's layer in *BCL2*-tg embryos is brought about through the increased tensional strain caused by the larger epiblast sizes in these embryos.

Is Rauber's Layer Disintegration Involved in Symmetry Breaking? The off-center thickening of part of the visceral hypoblast, seen from stage 3, marks the AVH and is the first morphological sign of symmetry breaking. The AVH expresses *CER1*. Examination of WT sectioned embryos (days 11 and 12, length range 0.3 mm to 1.3 mm) revealed no morphological evidence of hypoblast thickening in embryos with an intact Rauber's layer (8/8). Embryos with less than 30% of Rauber's layer gone (*SI Appendix*, Fig. S2 *A* and *B* and also figures 6C and 7B in ref. 19) either had no hypoblast thickening or, in two cases (*SI Appendix*, Fig. S2*C* and also figure 8D of ref. 19), the gap in Rauber's layer partially overlapped the AVH. This indicates that AVH formation is always initiated after the start of disintegration of Rauber's layer and raises the possibility that the initial site of Rauber's layer disintegration could be involved in AVH induction. Should RL disintegration indeed be necessary for AVH formation, it follows that, if Rauber's layer were maintained for longer than normal, as in the *BCL2* transgenic embryos, AVH formation would be delayed. We therefore stained *BCL2* and control transgenic embryos for the AVH marker *CER1*, focusing on four *BCL2* transgenic embryos in which Rauber's layer was still intact on day 13 (Fig. 4 *A*, *B*, and *E*). All of these showed asymmetric *CER1* expression and a thickened hypoblast, clearly indicating that formation of the AVH and thus initial symmetry breaking are not triggered by the disappearance of Rauber's layer. Furthermore, apart from one *BCL2* transgenic embryo in which *CER1* expression was located more toward the center of the embryonic disk, the *CER1* expression domain of *BCL2* embryos was very similar to that of the control transgenic embryos (Fig. 4*B*). The gaps in Rauber's layer were in no consistent positional relation to the underlying *CER1* expression (Fig. 4 *C* and *D*). We conclude that neither the timing nor positional commencement of Rauber's layer disintegration is involved in AVH formation or its eccentric localization.

Maintenance of RL Results in Ectopic *BRACHYURY* Expression. We next asked whether maintaining Rauber's layer for extended periods via BCL2 overexpression had any long-term patterning effects on the epiblast. To detect patterning changes, we assayed

for *BRACHYURY* (*BRA or "T"*) expression. *BRA* very specifically marks the posterior epiblast/embryonic ectoderm from just before endomesoderm cells are seen ingressing through the forming primitive streak (19) (Fig. 5*A*). In 6 of the 20 day 15, and 1 of the 3 day 17, *BCL2*-tg embryos (stages 4 and 5, pregastrulation to early gastrulation), ectopic expression of *BRA* was observed (Fig. 5 *B–J* and *SI Appendix*, Fig. S3). Embryos 1 to 3 showed two distinct adjacent regions of *BRA* suggestive of the formation of two distinct sites of gastrulation reminiscent of double axis formation (Fig. 5 *B–E*). Several embryos (#2, #5, and #7) showed ectopic patches of *BRA* expression near the anterior pole of the embryo (Fig. 5 *D* and *G–I*). The anterior extension of *BRA* expression across embryos with epiblast lengths ranging from 160 μm to 460 μm remained relatively constant, allowing for detection of outliers (Fig. 5*I*). Embryos 4 and 6 were notable in this respect, showing excessive anterior ectopic *BRA* expression (Fig. 5 *F*, *I*, and *J* and *SI Appendix*, Fig. S3), with embryo 4 (Fig. 5*F*) exhibiting persistence of Rauber's layer concomitant with the most extensive expression of *BRA*. Importantly, ectopic BRA expression is not correlated to epiblast size (Fig. 5 *I* and *J*), suggesting that this phenotype is caused by the persistence of Rauber's layer as opposed to the increased epiblast sizes seen upon BCL2 overexpression.

Discussion

Rauber's Layer Needs to Disappear in Cattle Embryos. We set out to determine whether the disappearance of Rauber's layer is a necessary event, by delaying its demise in cattle embryos. Our demonstration that Rauber's layer cells undergo apoptosis allowed us to employ a genetic strategy to achieve our goal. Generating transgenic embryos that overexpressed the anti-apoptotic protein BCL2 led to the maintenance of the polar trophoblast for 1 d longer than normal.

Somewhat unexpectedly, transgenic embryos exhibited an increase in epiblast size at all stages analyzed. Some of this size increase is likely to have been caused by *BCL2* overexpression preventing apoptosis in the epiblast. However, as, at any given time point, few epiblast cells are undergoing apoptosis (2%), apoptosis prevention can only partly explain the 20 to 35% increase in BCL2 epiblast size relative to WT or LacZ embryos, respectively, with the rest caused by an increase in cell proliferation. As BCL2 does not itself increase cell proliferation, but rather has a context-dependent antiproliferative effect (43), a proliferation-inducing effect would have to be indirect, potentially via the extended maintenance of Rauber's layer. Indeed, in mice, extraembryonic factors and signals diffusing into the epiblast are known to induce proliferation (32, 44, 45). Alternatively, the lengthened period of shielding the epiblast from potential antiproliferative maternal signals could have led to an increased epiblast size upon maintenance of Rauber's layer. This possibility, however, is unlikely, as the uterine milieu is designed to favor embryo growth, not inhibit it (46, 47). Either way, we conclude that, if Rauber's layer is not actively removed in a timely fashion, excessive epiblast proliferation may result.

More remarkably, however, extended culture of *BCL2*-overexpressing embryos to stages from just prior to the start of gastrulation resulted in embryos with ectopic domains of *BRA* expression, suggestive of supernumary gastrulation initiation sites and indicative of erroneous patterning of the embryonic ectoderm. These ectopic domains of *BRA* expression could have been caused by the increased size of the epiblast, by the delay in Rauber's layer disintegration, or by a combination of both factors. We believe the main cause is the delay in Rauber's layer disintegration, for two reasons. Firstly, day 15 epiblast sizes as well as epiblast to embryo length ratios show considerable variation in normal embryos, yet we have never observed such ectopic *Bra* domains (this work and ref. 19). Secondly, the ectopic *BRA* domains were also observed in BCL2 embryos with small epiblasts. This indicates that it is the extended survival of Rauber's layer that is primarily causative for this unique phenotype.

Lastly, maintaining Rauber's layer beyond its normal time span allowed us to unequivocally disprove the idea that the erratic breaking up of polar trophoblast in a Rauber's layer species such as cattle underlies the asymmetry of AVH establishment [first proposed by us in 2015 (19)]. Secondly, we had noted previously that, owing to the compact size of the epiblast in cattle, the cattle visceral hypoblast is unlikely to be under the influence of a DVH/AVH-inhibitory signal emanating either from the polar trophoblast, as happens in mice, or from the circumferential mural trophoblast, as may occur in rabbits, which have a relatively large embryonic disk (19). We now can conclude that, in cattle, the polar trophoblast indeed does not emit a

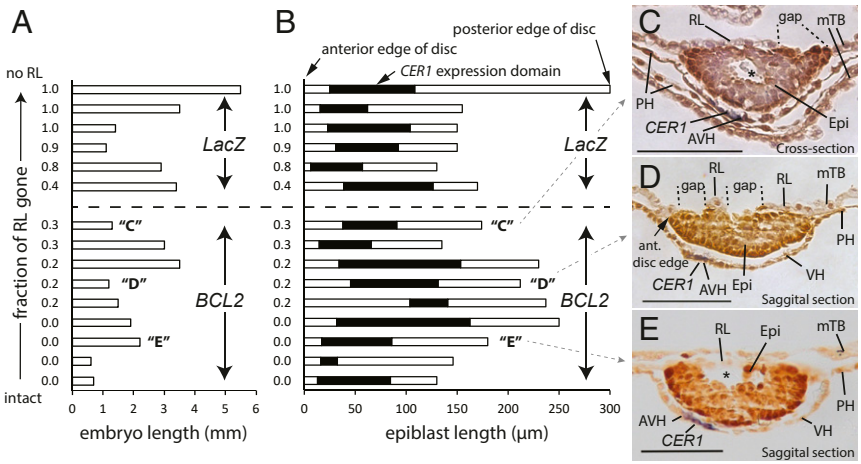

Fig. 4. Relationship of timing and positioning of gaps in Rauber's layer to that of the AVH as marked by CER1 mRNA. (*A* and *B*) Graphical display of transgenic control (top six) and *BCL2*-overexpressing (bottom nine) embryos displaying (*A*) embryo length or (*B*) embryonic disk/epiblast size horizontally (open box) with the anterior edge of the epiblasts aligned at the left, and *CER1* expression in the hypoblast superimposed (solid black). The degree of RL disintegration is shown for each embryo on the left, with embryos arranged from bottom to top in order of increasing (progressive) RL disintegration. Capital letters in parentheses denote embryos shown in adjacent panels. (*C–E*) Embryo sections of embryos "C" to "E" depicting the thickening of the *CER1*-expressing (blue staining) AVH, as well as gaps in RL. Sections have been stained post-WMISH with anti-OCT4 antibody (darker brown). PH, parietal hypoblast. Stars show cavities in the epiblast. Scale bar, 100 μm.

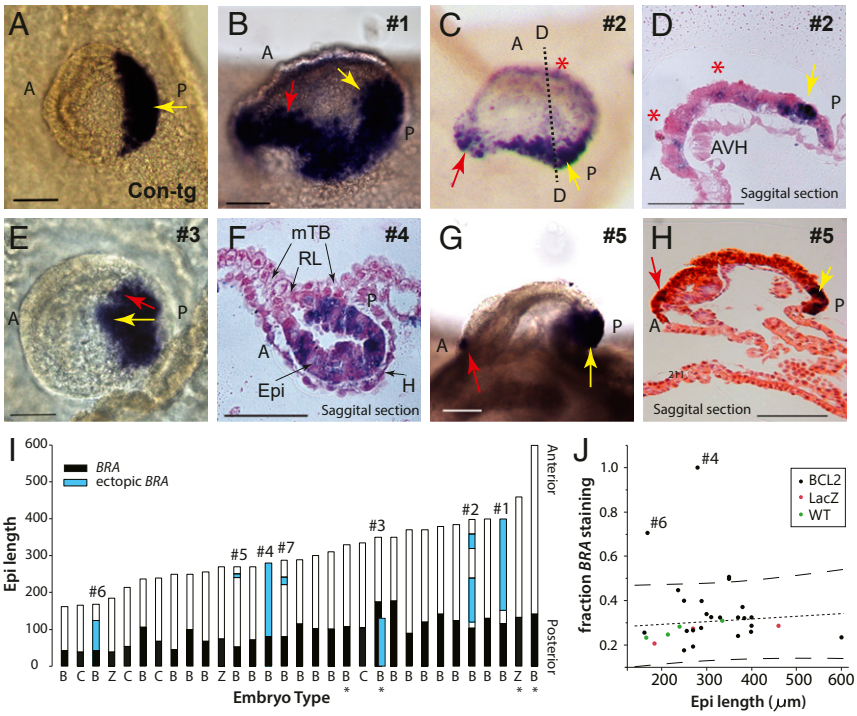

Fig. 5. BCL2 overexpression leads to ectopic domains of *Brachyury* expression. (*A–H*) WMISH for *BRA* (dark purple). (*A*) Control (*LacZ*-tg) embryo exhibiting typical posterior *BRA* staining (dorsal view). (*B*) Embryo #1 (oblique side view; posterior on right), (*C*) rear view and (*D*) saggital section (dotted line in *C*) of embryo #2, and (*E*) embryo #3 (dorsal view), all with two axes of Bra staining. Embryo 2 additionally exhibits anterior patches (red stars in *C* and *D*). (*F*) Embryo #4 with delayed epiblast flattening, expressing *BRA* throughout. (*G*) Side view and (*H*) saggital section of #5 with an ectopic anterior patch of staining. Yellow arrow, main axis; red arrow, presumptive secondary axis; A, anterior; mTB, mural trophoblast; P, posterior. (Scale bar, 100 μm.) (*I*) *BCL2-tg* ("B") and control ("Z", *LacZ-tg*; "C", WT) embryos arranged in increasing epiblast size (micrometers) with anterior to the top, *BRA* expression in black, and ectopic *BRA* expression in blue. The parallel bars for embryo #3 represent the two axes shown in *E*. Embryos are day 15 apart from four day 17 embryos (*). Labels (#) refer to embryos depicted in *B–H* and *SI Appendix*, Fig. S3. (*J*) Plot of the proportion of *BRA* staining along the anterior–posterior axis relative to epiblast size. The most conspicuous outliers are *BCL2-tg* embryos #4 and #6 (for sections, see *SI Appendix*, Fig. S3). Lines; regression with 95% CIs.

signal preventing AVH formation, as, even when maintaining Rauber's layer and thus any associated inhibitory influence for another full day, AVH formation and *CER1* expression are normal.

In summary, we have demonstrated that, in a Rauber's layer species, the disappearance of the polar trophectoderm is a regulated process that has to occur so that epiblast growth and *Brachyury* induction leading to gastrulation can proceed correctly. We contextualize these effects as follows.

Why Polar Trophoblast/Rauber's Layer Has to Disappear in Some Mammals but Not in Others. In a polar trophoblast-retaining mammal, namely, the mouse, this tissue is required for reciprocal interactions with the epiblast. In particular, *NODAL* mRNA is initially expressed all over the epiblast, but is refined to the proximal region due to an autoregulatory loop instigated by the limited diffusion of convertases from the trophoblast into the adjacent epiblast (48, 49). The convertases FURIN and PACE4 cleave PRONODAL protein to potentiate NODAL, which then signals to amplify its own transcription. NODAL additionally diffuses back into the adjacent trophoblast to maintain *BMP4* transcription (48). Secreted BMP, in turn, activates *WNT* transcription in the epiblast. WNT and the already activated NODAL then turn on genes required for gastrulation, including *BRA* (49–51). The reciprocal expression of these factors in adjacent tissues ensures that gastrulation commences only at the rim of the epiblast cup. Which side of the rim is dictated by the underlying visceral hypoblast which prevents gastrulation in the future anterior part of the epiblast via NODAL, BMP, and WNT inhibitors (CER, LEFTY, and DICKKOPF), secreted from the AVE (52). Notably, the same signaling pathways are also essential for gastrulation in another non-Rauber's layer species, namely, the human. Experiments involving micropatterned primed human embryonic stem cells suggested a key requirement for WNT and NODAL signaling in gastrulation/*BRA* activation, fueled by an exogenous supply (analogous to an extraembryonic source) of either BMP or WNT signals (53, 54).

Loss of function of key components of any these three (NODAL/BMP/WNT) pathways leads to an absence of *BRA*-positive mesoderm (25, 55, 56), but what relates particularly to our findings is that overstimulation of NODAL signaling (29), WNT signaling (57, 58), or BMP signaling (59) leads to ectopic domains of *BRA* and/or resulting secondary axes in mice. This phenotype is similar to that seen in our *BCL2*-transgenic cattle embryos. We thus posit that maintaining Rauber's layer results in mislocalized activation of either the NODAL, BMP, or WNT signaling network, leading to ectopic *BRA* expression.

An evolutionary parsimonious explanation for the observed phenotype is that Rauber's layer, being polar trophoblast, is inherently equivalent (see Introduction) to the persistent polar trophoblast (extraembryonic ectoderm) of the mouse. Thus Rauber's layer would be able to vertically signal to the underlying epiblast wherever these tissues are in close proximity. However, in cattle embryos—and all other Rauber's layer species—such signaling presents a problem, because the ICM develops into a pseudostratified epiblast epithelium and thus is adjacent over its entire surface to the polar trophoblast. Thus it would not be able to escape signals from a persisting polar trophoblast layer, which

would lead to widespread, instead of epiblast-edge localized, activation of reciprocal NODAL/BMP/WNT signaling networks (Fig. 6*A*).

How then do polar trophoblast-maintaining species prevent ectopic *BRA* activation? We suggest that these species evolved another solution: the formation of a proamniotic cavity within the epiblast. Such a cavity interposes its roof (the amniotic ectoderm) between the polar trophoblast and the epiblast floor, effectively preventing reciprocal vertical signaling between the central epiblast and trophoblast (green asterisk in Fig. 6 *B*, *Middle*). In mouse and rat embryos, the proamniotic cavity fuses with cavities developing within the extraembryonic ectoderm to form a hollowed out egg cylinder structure, now containing a trophoblast "roof" (Fig. 6 *B*, *Bottom*). In this variation, there is no amniotic roof shielding the central epiblast, but the elongated shape of the proamniotic cavity distances the apex (center) of the epiblast from the extraembryonic ectoderm, preventing vertical signaling between these regions (green asterisk in Fig. 6 *B*, *Bottom*).

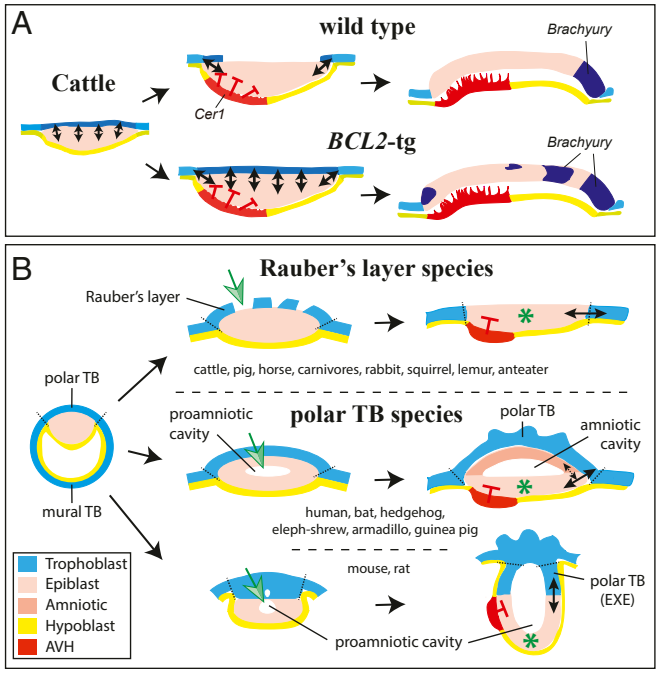

Fig. 6. Model explaining effect of maintaining Rauber's layer in cattle and the relationship between trophoblast and epiblast signaling in eutherian mammals. (*A*) Model showing how extended signaling interactions over all of the epiblast occur when the polar trophoblast (Rauber's layer) is maintained as in *BCL2*-trasgenic cattle embryos. This is proposed to lead, via epiblast–trophoblast boundary-dependent signaling circuit(s) to *BRA-CHYURY* induction. (*B*) Eutherian mammalian development showing the two major mechanisms (green arrow) for ensuring that trophoblast–epiblast interactions (solid double arrows) leading to gastrulation induction are restricted to the boundary of the epiblast. A green asterisk marks this signal-free epiblast center (apex for cup-shaped epiblast). In Rauber's layer species (*Top*), no proamniotic cavity is formed, although epiblast cavitation may occur. The amniotic cavity is formed after gastrulation has commenced via a folding mechanism (64). In species retaining the polar trophoblast (*Middle* and *Bottom*), the proamniotic epiblast cavity usually develops into the future amniotic cavity (*Middle*). In some of these species (higher primates, some bats, guinea pigs), the epiblast is distanced from all trophoblast via hypoblast interpolation (not shown). In such cases, the amniotic ectoderm–epiblast border may replace the function of the prior trophoblast–epiblast border (stippled arrow in *Middle*). In some polar TB species, such as mouse and rat (*Bottom*), the proamniotic cavity fuses with trophoblast cavities. The amniotic cavity is partitioned off this epiblast- and trophoblast-enclosed cavity after gastrulation has commenced (65).

In line with our suggestion, we discovered a hitherto unnoticed division in development among eutherian mammals (*SI Appendix*, Table S1). All Rauber's layer species (which lose polar trophoblast) do not form a proamniotic cavity, even though they may show signs of epiblast cavitation during the epiblast transition to a pseudostratified epithelium (see, for example, asterisk in Fig. 4). They, consequently, always form the amniotic cavity secondarily, after gastrulation has commenced. All other mammals (polar trophoblast species) retain the polar trophoblast and form a prominent proamniotic cavity which, in many of these species, develops into the amniotic cavity (*SI Appendix*, Table S1).

This correlation, in combination with our data using transgenic cattle embryos, leads us to the interpretation that proamniotic cavity formation is predominantly an adaptation for preventing inappropriate polar trophoblast signaling in animals that have a need for maintaining the polar trophoblast.

One further point should be noted. Epiblast cavitation divides the epiblast into two territories, the embryonic epiblast (embryonic ectoderm) and the amniotic ectoderm, joined only at their rims, not unlike the trophoblast–epiblast configuration that is seen at gastrulation induction stages. Thus, in some polar trophoblast species, such as higher primates (60), some bats (9), and guinea pigs (61), where hypoblast derivatives separate the epiblast from contact-dependent trophoblast interactions, this novel epiblast/amnion boundary may substitute for the gastrulation inductive function of the epiblast/trophoblast boundary. Evidence for this idea comes from 1) cynomolgus monkeys (macaques), that express one of the key mouse extraembryonic ectoderm genes involved in gastrulation (and germ cell) induction, *BMP4,* in the amniotic ectoderm (60), and 2) in human embryoid microfluidic culture systems, where gastrulation and germ cell induction can be induced in the absence of trophoblast tissue (62).

Materials and Methods

Embryo Generation and Embryo Powder. Animal work was carried out under animal ethics approval Ruakura Animal Ethics Committee 12025 (Hamilton, New Zealand), and all efforts were made to minimize animal suffering. Embryos were generated and recovered as described previously (19). Somatic cell nuclear transfer embryos were generated as previously described (37). Embryos were genotyped using GFP and LacZ primers as previously described (36). Embryo powder was made from day 15 elongated embryos by vigorous pipetting in a minimal volume of phosphate-buffered saline (PBS), addition of four volumes of ice-cold acetone, vortexing, then leaving on ice for 30 min. The sample was centrifuged 10 min at 13,000 × *g*, and the pellet was treated again with acetone as before. After recentrifugation, the pellet was placed on a sheet of filter paper (Grade 1, Whatman), gently ground with a small ceramic pestle, air dried, and stored at 4 °C.

WMISH and Immunohistochemistry. Whole-mount in situ hybridization (WMISH) was carried out as previously described (19). To enable better visualization and orientation of the embryonic disk, following WMISH, some embryos were stained with OCT4 antibody. Embryos were washed in PBS and 0.1% Triton X-100, permeabilized in 1% Triton X-100/PBS for 15 min, blocked 1 h in PBS/0.1% triton/5% lamb serum (heat treated), and incubated overnight at 4 °C with a 1/250 dilution of OCT4 antibody (Santa Cruz sc-9081). Embryos were washed and stained as described (*SI Appendix, Supplementary Information Materials and Methods*) for the proliferation assay.

Generation of the pGFP-2A-BCL2iP-CAG Plasmid. Bovine *BCL2* (NM_001166486.1) was PCR amplified from day 20 cattle embryo complementary DNA (cDNA) using *AscI-2A-Bcl2*-f (5′-AA*GGGCGCGCC*-AGGCAGTGGAGAGGGCAGAGGAAG TCTGCTAACATGCGGTGACGTCGAGGAGAA-TCCTGGCCCA-ATGGCGCACGCGGGG GGAACAGGCTA) and *NotI-BCL2*-r primers (5′-GGG*GCGGCCGC*-TCACTTATGGCC CAGATAGGCA) and inserted, via standard restriction and ligation procedures, into the *AscI* and *NotI* sites of *pCAGiPmod*, derived by replacing the EcoRI/NotI stuffer region of *pPyCAGiP* (63) with a multiple cloning region *GAATTC-ATTTAAA T-tGGCGCGCC-CTCGAG-AGATCT-GCTAGC-aaGCGGCCGC*. Emerald GFP with an upstream KOZAK sequence was then inserted into the *EcoRI/AscI* sites upstream of the *BCL2* fragment of this plasmid. The *GFP*-containing fragment was PCR amplified from *pcDNA6.2-GW-GFP-miR* (Invitrogen)

using primers *EcoRI*-KOZAK-*EmGFP*-f (5′-AAA*GAATTC*-CACCATGGTGAGC AAGGGCGAGGAG) and *AscI*-GFP-r (5′- CCT*GGCGCGCC*CCTTGTACAGCTC GTCCATGCCG).

Transgenic Cell Lines. Primary bovine female embryonic fibroblast cells (EF5) were stably transfected with *pGFP-2A-BCL2iP-CAG* using Lipofectamine-2000 according to the manufacturer's instructions (Life Technologies), and individual colonies were picked and expanded after Puromycin selection and karyotyped according to standard procedures. The pCAG-LacZiPuro control cell lines have been previously described (36).

Expression Analysis. Total mRNA from cell lines and trophoblast fragments obtained by microsurgery were extracted using TRIzol, then DNaseI digested, reverse transcribed, and used for real-time RT-PCR as previously described (37). The primer pair BCL2-3′UTR (5′-ACGGAGGCTG-GGACGCCTTT, 5′-CAG TGGTGCA-TCAGCAACAATGC, 229 base pairs [bp]) were used to measure endogenous expression, as this region was not included in the transgenic *BCL2* vector and BCL2 coding (5′-GGGCGCATCG-TGGCCTTCTT, 5′-CAGGGT GATG-CAAGCGCCCA, 269 bp) to measure total *BCL2* expression. *ASCL2* and the three housekeeping primer sets were previously described (37).

Cell Proliferation and Apoptotic Assays. Whole-mount cell proliferation in cattle embryos was measured using anti–phospho-Histone H3 Ab (#06-570 Upstate Biotechnologies), and apoptosis was measured in embryos and cell lines using active caspase 3 antibody (9661, Cell Signaling Technology), as described in detail (*SI Appendix*, *Supplementary Information Materials and Methods*).

Statistical Analysis. Statistical analyses of the types mentioned in the text and figures were done using GenStat statistical software (VSN International).

Data Availability Statement. All data are included in the paper or *SI Appendix*.

ACKNOWLEDGMENTS. This work was supported by Royal Society of New Zealand Grant 07-AGR-004 as well as Victoria University of Wellington Grant 8-1620-222123 awarded to P.L.P., and Grant C10X1001 and AgResearch CORE funding, from the Ministry of Business and Innovation. We thank Dr. Craig S. Smith and Harold Henderson for advice on gene expression and statistical analyses, respectively, Martin Berg for embryo transfers and flushings, and members of the Reproductive Technologies team for help with nuclear transfers. We thank Dr. Craig S. Smith for critical reading of the manuscript.

1. H. W. Mossman, Comparative morphogenesis of the fetal membranes and accessory uterine structures. *Contrib. Embryol.* **26**, 133–137 (1937).
2. A. Rauber, Die erste Entwicklung des Kaninchens. *Sitzungsber. Naturfor. Gesell. Leipzig* **10**, 103–109 (1875).
3. A. Koellicker, Die Entwickelung der Keimblatter des Kaninchens. *Zool. Anz.* **3**, 370–375 (1880).
4. R. L. Gardner, M. H. Johnson, An investigation of inner cell mass and trophoblast tissues following their isolation from the mouse blastocyst. *J. Embryol. Exp. Morphol.* **28**, 279–312 (1972).
5. E. B. Ilgren, The control of trophoblastic growth in the guinea pig. *J. Embryol. Exp. Morphol.* **60**, 405–418 (1980).
6. A. C. Enders, S. Schlafke, Differentiation of the blastocyst of the rhesus monkey. *Am. J. Anat.* **162**, 1–21 (1981).
7. A. T. Hertig, J. Rock, E. C. Adams, A description of 34 human ova within the first 17 days of development. *Am. J. Anat.* **98**, 435–493 (1956).
8. W. P. Luckett, Origin and differentiation of the yolk sac and extraembryonic mesoderm in presomite human and rhesus monkey embryos. *Am. J. Anat.* **152**, 59–97 (1978).
9. J. J. Rasweiler 4th, Reproduction in the long-tongued bat, *Glossophaga soricina*. II. Implantation and early embryonic development. *Am. J. Anat.* **139**, 1–35 (1974).
10. W. J. Bleier, Early embryology and implantation in the California leaf-nosed bat, *Macrotus californicus*. *Anat. Rec.* **182**, 237–253 (1975).
11. M. van der Merwe, Histological study of implantation in the Natal clinging bat (*Miniopterus schreibersii natalensis*). *J. Reprod. Fertil.* **65**, 319–323 (1982).
12. R. L. Gardner, V. E. Papaioannou, S. C. Barton, Origin of the ectoplacental cone and secondary giant cells in mouse blastocysts reconstituted from isolated trophoblast and inner cell mass. *J. Embryol. Exp. Morphol.* **30**, 561–572 (1973).
13. M. Donnison *et al*., Loss of the extraembryonic ectoderm in Elf5 mutants leads to defects in embryonic patterning. *Development* **132**, 2299–2308 (2005).
14. B. S. Williams, J. D. Biggers, Polar trophoblast (Rauber's layer) of the rabbit blastocyst. *Anat. Rec.* **227**, 211–222 (1990).
15. A. C. Enders, K. C. Lantz, I. K. Liu, S. Schlafke, Loss of polar trophoblast during differentiation of the blastocyst of the horse. *J. Reprod. Fertil.* **83**, 447–460 (1988).
16. M. Vejlsted *et al*., Ultrastructural and immunohistochemical characterization of the bovine epiblast. *Biol. Reprod.* **72**, 678–686 (2005).
17. P. M. Barends *et al*., Integrity of the preimplantation pig blastocyst during expansion and loss of polar trophectoderm (Rauber cells) and the morphology of the embryoblast as an indicator for developmental stage. *J. Reprod. Fertil.* **87**, 715–726 (1989).
18. J. E. Flechon, Morphological aspects of embryonic disc at the time of its appearance in the blastocyst of farm mammals. *Scan. Electron Microsc.* **11**, 541–547 (1978).
19. J. van Leeuwen, D. K. Berg, P. L. Pfeffer, Morphological and gene expression changes in cattle embryos from hatched blastocyst to early gastrulation stages after transfer of in vitro produced embryos. *PLoS One* **10**, e0129787 (2015).
20. G. Valdez Magaña, A. Rodríguez, H. Zhang, R. Webb, R. Alberio, Paracrine effects of embryo-derived FGF4 and BMP4 during pig trophoblast elongation. *Dev. Biol.* **387**, 15–27 (2014).
21. R. Hassoun, P. Schwartz, K. Feistel, M. Blum, C. Viebahn, Axial differentiation and early gastrulation stages of the pig embryo. *Differentiation* **78**, 301–311 (2009).
22. C. Hopf, C. Viebahn, B. Püschel, BMP signals and the transcriptional repressor BLIMP1 during germline segregation in the mammalian embryo. *Dev. Genes Evol.* **221**, 209–223 (2011).
23. M. Yoshida *et al*., Conserved and divergent expression patterns of markers of axial development in eutherian mammals. *Dev. Dyn.* **245**, 67–86 (2016).
24. S. A. Degrelle *et al*., Molecular evidence for a critical period in mural trophoblast development in bovine blastocysts. *Dev. Biol.* **288**, 448–460 (2005).
25. F. L. Conlon *et al*., A primary requirement for nodal in the formation and maintenance of the primitive streak in the mouse. *Development* **120**, 1919–1928 (1994).
26. K. A. Lawson *et al*., Bmp4 is required for the generation of primordial germ cells in the mouse embryo. *Genes Dev.* **13**, 424–436 (1999).
27. J. A. Belo *et al*., Cerberus-like is a secreted factor with neutralizing activity expressed in the anterior primitive endoderm of the mouse gastrula. *Mech. Dev.* **68**, 45–57 (1997).
28. P. Thomas, R. Beddington, Anterior primitive endoderm may be responsible for patterning the anterior neural plate in the mouse embryo. *Curr. Biol.* **6**, 1487–1496 (1996).
29. A. Perea-Gomez *et al*., Nodal antagonists in the anterior visceral endoderm prevent the formation of multiple primitive streaks. *Dev. Cell* **3**, 745–756 (2002).
30. K. Takaoka, M. Yamamoto, H. Hamada, Origin and role of distal visceral endoderm, a group of cells that determines anterior-posterior polarity of the mouse embryo. *Nat. Cell Biol.* **13**, 743–752 (2011).
31. T. A. Rodriguez, S. Srinivas, M. P. Clements, J. C. Smith, R. S. Beddington, Induction and migration of the anterior visceral endoderm is regulated by the extra-embryonic ectoderm. *Development* **132**, 2513–2520 (2005).
32. D. Mesnard, M. Guzman-Ayala, D. B. Constam, Nodal specifies embryonic visceral endoderm and sustains pluripotent cells in the epiblast before overt axial patterning. *Development* **133**, 2497–2505 (2006).
33. A. A. W. Hubrecht, Studies in mammalian embryology, II. The development of the germinal layers of *Sorex vulgaris*. *Q. J. Microsc. Sci.* **31**, 499–568 (1890).
34. C. Viebahn, B. Mayer, M. Hrabé de Angelis, Signs of the principle body axes prior to primitive streak formation in the rabbit embryo. *Anat. Embryol. (Berl.)* **192**, 159–169 (1995).
35. P. Maddox-Hyttel *et al*., Immunohistochemical and ultrastructural characterization of the initial post-hatching development of bovine embryos. *Reproduction* **125**, 607–623 (2003).
36. D. K. Berg *et al*., Trophectoderm lineage determination in cattle. *Dev. Cell* **20**, 244–255 (2011).
37. J. van Leeuwen, D. K. Berg, C. S. Smith, D. N. Wells, P. L. Pfeffer, Specific epiblast loss and hypoblast impairment in cattle embryos sensitized to survival signalling by ubiquitous overexpression of the proapoptotic gene BAD. *PLoS One* **9**, e96843 (2014).
38. M. L. L. Donnelly *et al*., Analysis of the aphthovirus 2A/2B polyprotein "cleavage" mechanism indicates not a proteolytic reaction, but a novel translational effect: A putative ribosomal "skip.". *J. Gen. Virol.* **82**, 1013–1025 (2001).
39. C. S. Smith, D. K. Berg, M. Berg, P. L. Pfeffer, Nuclear transfer-specific defects are not apparent during the second week of embryogenesis in cattle. *Cell. Reprogram.* **12**, 699–707 (2010).
40. D. K. Berg, J. van Leeuwen, S. Beaumont, M. Berg, P. L. Pfeffer, Embryo loss in cattle between days 7 and 16 of pregnancy. *Theriogenology* **73**, 250–260 (2010).
41. K. J. Betteridge, M. D. Eaglesome, G. C. B. Randall, D. Mitchell, Collection, description and transfer of embryos from cattle 10–16 days after oestrus. *J. Reprod. Fertil.* **59**, 205–216 (1980).
42. P. L. Pfeffer, C. S. Smith, P. Maclean, D. K. Berg, Gene expression analysis of bovine embryonic disc, trophoblast and parietal hypoblast at the start of gastrulation. *Zygote* **25**, 265–278 (2017).
43. S. Zinkel, A. Gross, E. Yang, BCL2 family in DNA damage and cell cycle control. *Cell Death Differ.* **13**, 1351–1359 (2006).
44. D. W. Stuckey *et al*., Coordination of cell proliferation and anterior-posterior axis establishment in the mouse embryo. *Development* **138**, 1521–1530 (2011).
45. A. Di-Gregorio *et al*., BMP signalling inhibits premature neural differentiation in the mouse embryo. *Development* **134**, 3359–3369 (2007).
46. L. Blomberg, K. Hashizume, C. Viebahn, Blastocyst elongation, trophoblastic differentiation, and embryonic pattern formation. *Reproduction* **135**, 181–195 (2008).
47. P. Lonergan, N. Forde, T. Spencer, Role of progesterone in embryo development in cattle. *Reprod. Fertil. Dev.* **28**, 66–74 (2016).
48. N. Ben-Haim *et al*., The nodal precursor acting via activin receptors induces mesoderm by maintaining a source of its convertases and BMP4. *Dev. Cell* **11**, 313–323 (2006).
49. J. Brennan *et al*., Nodal signalling in the epiblast patterns the early mouse embryo. *Nature* **411**, 965–969 (2001).
50. N. S. Funa *et al*., β-Catenin regulates primitive streak induction through collaborative interactions with SMAD2/SMAD3 and OCT4. *Cell Stem Cell* **16**, 639–652 (2015).

51. T. P. Yamaguchi, S. Takada, Y. Yoshikawa, N. Wu, A. P. McMahon, T (Brachyury) is a direct target of Wnt3a during paraxial mesoderm specification. *Genes Dev.* **13**, 3185–3190 (1999).
52. K. Takaoka, H. Hamada, Cell fate decisions and axis determination in the early mouse embryo. *Development* **139**, 3–14 (2012).
53. A. Warmflash, B. Sorre, F. Etoc, E. D. Siggia, A. H. Brivanlou, A method to recapitulate early embryonic spatial patterning in human embryonic stem cells. *Nat. Methods* **11**, 847–854 (2014).
54. I. Martyn, T. Y. Kanno, A. Ruzo, E. D. Siggia, A. H. Brivanlou, Self-organization of a human organizer by combined Wnt and Nodal signalling. *Nature* **558**, 132–135 (2018).
55. P. Liu *et al*., Requirement for Wnt3 in vertebrate axis formation. *Nat. Genet.* **22**, 361–365 (1999).
56. G. Winnier, M. Blessing, P. A. Labosky, B. L. Hogan, Bone morphogenetic protein-4 is required for mesoderm formation and patterning in the mouse. *Genes Dev.* **9**, 2105–2116 (1995).
57. H. Pöpperl *et al*., Misexpression of Cwnt8C in the mouse induces an ectopic embryonic axis and causes a truncation of the anterior neuroectoderm. *Development* **124**, 2997–3005 (1997).
58. B. J. Merrill *et al*., Tcf3: A transcriptional regulator of axis induction in the early embryo. *Development* **131**, 263–274 (2004).
59. P. N. Pereira *et al*., Antagonism of Nodal signaling by BMP/Smad5 prevents ectopic primitive streak formation in the mouse amnion. *Development* **139**, 3343–3354 (2012).
60. K. Sasaki *et al*., The germ cell fate of cynomolgus monkeys is specified in the nascent amnion. *Dev. Cell* **39**, 169–185 (2016).
61. A. A. W. Hubrecht, Studies in mammalian embryology. I. The placentation of *Erinaceus europaeus*, with remarks on the phylogeny of the placenta. *Q. J. Microsc. Sci.* **30**, 283–404 (1889).
62. Y. Zheng *et al*., Controlled modelling of human epiblast and amnion development using stem cells. *Nature* **573**, 421–425 (2019).
63. I. Chambers *et al*., Functional expression cloning of Nanog, a pluripotency sustaining factor in embryonic stem cells. *Cell* **113**, 643–655 (2003).
64. J. S. Greenstein, R. C. Foley, Early embryology of the cow. I. Gastrula and primitive streak stages. *J. Dairy Sci.* **41**, 409–421 (1958).
65. P. N. Pereira *et al*., Amnion formation in the mouse embryo: The single amniochorionic fold model. *BMC Dev. Biol.* **11**, 48 (2011).